Sensors & Diagnostics

PAPER

View Article Online
View Journal | View Issue



Cite this: *Sens. Diagn.*, 2024, **3**, 1062

# An imidazo[1,2-*a*]pyridine-functionalized xanthene fluorescent probe for naked-eye detection of $Hg^{2+}$ and its application in cell imaging and test strips†

Xu-Hong Han,[a] Piao Zhao,[a] Meng-Ke Tang,[b] Lei Yang,[b] Qing Wang *[b] and Shu-Sheng Zhang *[b]

Received 23rd March 2024,
Accepted 27th April 2024

DOI: 10.1039/d4sd00090k

rsc.li/sensors

An imidazo[1,2-*a*]pyridine-functionalized xanthene dye (**Rh-Ip**) was designed and developed as a fluorescent probe (**Rh-Ip-Hy**) for $Hg^{2+}$ by introducing spirolactam to the molecule. The probe **Rh-Ip-Hy** with a ring-closed spirolactam structure reacts with $Hg^{2+}$ to form a fluorescent ring-opened spirolactone structure. Due to its asymmetric structure and the presence of a Lewis base site, the probe exhibits a larger Stokes shift and higher pH tolerance than the traditional xanthene dyes and probes. Furthermore, the probe is highly selective to $Hg^{2+}$ within a wide pH range of 5.0–11.0. The probe **Rh-Ip-Hy** also exhibits low cytotoxicity and can be used for the detection of $Hg^{2+}$ in living HeLa cells through fluorescence imaging. Finally, a paper-based test strip was prepared and successfully applied for the detection of $Hg^{2+}$ in tap water and lake water samples.

## Introduction

Mercury is a highly toxic pollutant that poses a significant threat to the environment. Mercury, even when present in low concentrations in the environment, can accumulate through the food chain,[1,2] leading to a variety of diseases, including neurological damage[3] and serious cognitive and motion disorders.[4] Therefore, it is important to develop simple tools for the sensitive and selective detection of $Hg^{2+}$ in various water samples.

Over the past decades, several methods such as high-performance liquid chromatography, atomic emission spectroscopy, surface-enhanced Raman spectroscopy, and inductively coupled plasma mass spectroscopy have been developed for detecting $Hg^{2+}$ in environmental samples with high sensitivity, selectivity, and precision.[5,6] However, most of these methods are time-consuming or need tedious sample preparation steps, for which reason they are not suitable for on-site analysis and *in vivo* imaging.[7] Fluorescent probe-based detection methods have been widely used for detecting various analytes both *in vitro* and *in vivo* because of their advantages such as high selectivity and sensitivity, non-invasiveness and high spatiotemporal resolution.[8–14]

Due to their advantages including high molar absorption coefficient, high fluorescence quantum yield, and good photostability, xanthene-based fluorophores including rhodamines and fluoresceins have been widely used for designing fluorescent probes by following a target-induced ring-opening strategy enabled by the unique property of spirolactam.[15–17] Initially, these probes are in the spirolactam form, which is nonfluorescent and colourless. However, in the presence of analytes, strong fluorescence and significant colour changes are observed because of the analyte-triggered ring-opening of probes. Although various xanthene-based probes have been developed for detecting $Hg^{2+}$ with high selectivity and sensitivity, there are still some limitations to these probes. For example, classic rhodamine and fluorescein dyes have a small Stokes shift of 20–40 nm,[18,19] which is susceptible to being affected by self-absorption and background fluorescence. Furthermore, some reported spirolactam-based probes are vulnerable to $H^+$ (see Table S1; ESI†), causing undesired background signals, which may impede their applications to practical complex samples and *in vivo* imaging (Scheme 1).[20,21] These concerns encouraged us to develop a novel fluorescent probe for detecting $Hg^{2+}$ in various aquatic environments.

In the present manuscript, an imidazo[1,2-*a*]pyridine group is grafted to a xanthene plane to form a probe with an asymmetrical structure and a Lewis base site. The aim is to increase the Stokes shifts and improve the pH tolerance. As expected, the $Hg^{2+}$ fluorescent probe (**Rh-Ip-Hy**) exhibits a

[a] *College of Chemistry and Chemical Engineering, Linyi University, Linyi 276005, PR China*
[b] *Shandong Provincial Key Laboratory of Detection Technology for Tumor Markers, School of Medicine, Linyi University, Linyi 276005, PR China.*
*E-mail: qing1016.hi@163.com, shushzhang@126.com*

† Electronic supplementary information (ESI) available: Copies of $^1H/^{13}C$ NMR and HRMS spectra for **Rh-Ip** and **Rh-Ip-Hy**, the limit of detection, HRMS spectra of sensing mechanism are included. See DOI: https://doi.org/10.1039/d4sd00090k

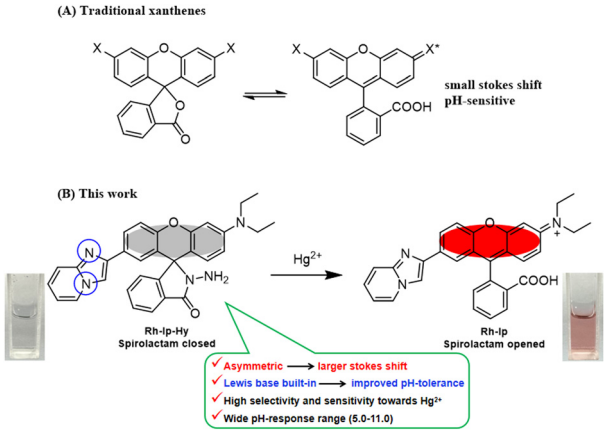


**Scheme 1** (A) Structures of traditional xanthenes. (B) Structures and color changes of **Rh-Ip-Hy** (5 μM) before and after exposure to $Hg^{2+}$ (50 μM).

large Stokes shift (75 nm) in the presence of $Hg^{2+}$ and high pH tolerance within the pH range of 1–14. Furthermore, the proposed probe **Rh-Ip-Hy** is highly selective and sensitive to $Hg^{2+}$ within a wide pH range (5.0–11.0), and can be utilized for the quantitative detection of $Hg^{2+}$ in living HeLa cells.

# Experimental

### Materials and instrumentation

All chemicals and reagents were purchased from Innochem Company (Beijing, China) and used without further treatment unless noted. Test solutions of $Zn(NO_3)_2$, $Cu(NO_3)_2$, $AgNO_3$, $Al(NO_3)_3{\cdot}9H_2O$, NaCl, $FeCl_2$, $FeCl_3$, KCl, LiCl, $CaCl_2{\cdot}2H_2O$, $BaCl_2{\cdot}2H_2O$, $MgSO_4$, $Ni(ClO_4)_2$, $Mn(ClO_4)_2$, $Cd(ClO_4)_2$, $Co(ClO_4)_2$, and $Pb(CH_3COO)_2$ were prepared by dissolving or diluting these compounds in double-distilled water, followed by further dilution if necessary.

### Instrumentation and spectroscopic studies

Absorption spectra were recorded on an Agilent Cary 60 spectrophotometer. Fluorescence spectroscopy was conducted on a Hitachi F-4600 spectrometer. $^1$H NMR (400 MHz) and $^{13}$C NMR (100 MHz) spectra were recorded on a Bruker AVANCE III 400 MHz spectrometer with chemical shifts reported in ppm (TMS as the internal standard). High-resolution mass spectrometry (HRMS) was performed with an Agilent 6510 Q-TOF LC/MS instrument (Agilent Technologies, Palo Alto, USA) that was equipped with an electrospray ionization (ESI) source. The pH measurements were carried out using a Leici PHS-3C meter. Cells were imaged using a TCS SP8 II confocal laser scanning microscope (Nikon C2plus, Germany).

### Sample preparation

The stock solution of **Rh-Ip-Hy** (10 mM) was prepared in *N*,*N*-dimethylformamide (DMF). The test solution was set at a concentration of 5 μM by diluting the stock solution with $H_2O$/EtOH (v/v; 4/1). Stock solutions of various metal ions (10.0 mM) were prepared in distilled water and were diluted with $H_2O$/EtOH (v/v; 4/1) to the required concentration for specific experiments. The emission spectra were recorded 30 min after the addition of each analyte.

### Synthesis of the dye Rh-Ip

A mixture of compound **1** (ref. 22) (1.2 g, 5 mmol) and 2-[4-(diethylamino)-2-hydroxybenzoyl]benzoic acid (1.4 g, 4.47 mmol) was dissolved in $CF_3COOH/CH_3SO_3H$ (20 mL, v/v = 1/1). The resulting solution was heated at 80 °C for 24 h. After cooling, the mixture was poured into $H_2O$ (80 mL), neutralized using $NaHCO_3$, and extracted with $CH_2Cl_2$ (40 mL × 3). Then, the organic layer was dried over $Na_2SO_4$. The solvent was removed under reduced pressure. The final product was purified using column chromatography (PE/EtOAc = 2/1) to afford the target compound as a brown solid (762 mg, yield: 35%). HRMS: *m*/*z* [M + $H^+$] = 488.1973, [M + 2$H^+$] = 244.6021; calcd for [$C_{31}H_{25}N_3O_3$ + $H^+$]: 488.1974, [$C_{31}H_{25}N_3O_3$ + 2$H^+$]: 244.6053. $^1$H NMR (400 MHz, $CDCl_3$, ppm): $\delta$ 1.16 (t, 6H, $J$ = 7.0 Hz, –$CH_3$), 3.34 (q, 4H, $J$ = 7.0 Hz, –$CH_2$), 6.34 (dd, 1H, $J$ = 8.8 Hz, 2.8 Hz, Ar–H), 6.45 (d, 1H, $J$ = 2.8 Hz, Ar–H), 6.56 (d, 1H, $J$ = 8.8 Hz, Ar–H), 6.71 (t, 1H, $J$ = 7.0 Hz, Ar–H), 7.10 (t, 1H, $J$ = 7.0 Hz, Ar–H), 7.19 (d, 1H, $J$ = 7.2 Hz, Ar–H), 7.24 (d, 1H, $J$ = 6.8 Hz, Ar–H), 7.31 (d, 1H, $J$ = 8.4 Hz, Ar–H), 7.53 (d, 1H, $J$ = 9.2 Hz, Ar–H), 7.59 (m, 3H, Ar–H), 8.01 (m, 3H, Ar–H). $^{13}$C NMR (100 MHz, $CDCl_3$, ppm): $\delta$ 12.64, 44.60, 84.06, 97.81, 105.31, 108.02, 108.62, 112.59, 117.39, 117.66, 119.73, 124.21, 124.86, 125.11, 125.55, 125.65, 127.01, 128.60, 128.85, 129.37, 129.62, 135.06, 144.70, 145.58, 149.76, 151.699, 152.77, 153.59, 169.93.

**Synthesis of Rh-Ip-Hy.** To an ethanolic solution (10 mL) of **Rh-Ip** (250 mg, 0.51 mmol), hydrazine hydrate (1 mL) was added. The mixture was heated at 100 °C for 4 h. After cooling, the solvent was removed under reduced pressure. The residue was purified by column chromatography ($CH_2Cl_2/C_2H_5OH$ = 100/1) to afford the target compound as a pale brown solid (128 mg, yield: 50%). HRMS: *m*/*z* [M + $H^+$] = 502.2238, [M + 2$H^+$] = 251.6155; calcd for [$C_{31}H_{27}N_5O_2$ + $H^+$]: 502.2238, [$C_{31}H_{27}N_5O_2$ + 2$H^+$]: 251.6155. $^1$H NMR (400 MHz, $CDCl_3$, ppm, contain $H_2O$): $\delta$ 1.18 (t, 6H, $J$ = 7.0 Hz, –$CH_3$), 3.35 (q, 4H, $J$ = 7.0 Hz, –$CH_2$), 3.79 (s, 2H, –$NH_2$), 6.33 (dd, 1H, $J$ = 8.8 Hz, 2.4 Hz, Ar–H), 6.47 (d, 1H, J = 2.4 Hz, Ar–H), 6.49 (d, 1H, $J$ = 8.8 Hz, Ar–H), 6.73 (t, 1H, $J$ = 7.8 Hz, Ar–H), 7.12 (t, 2H, $J$ = 7.8 Hz, Ar–H), 7.21 (d, 1H, $J$ = 2.0 Hz, Ar–H), 7.31 (dd, 1H, $J$ = 8.4 Hz, 2.0 Hz, Ar–H), 7.45–7.55 (m, 3H, Ar–H), 7.64 (d, 1H, $J$ = 8.4 Hz, Ar–H), 7.95–7.99 (m, 2H, Ar–H), 8.02 (d, 1H, $J$ = 6.8 Hz, Ar–H). $^{13}$C NMR (100 MHz, $CDCl_3$, ppm): $\delta$ 12.67, 44.48, 65.99, 98.28, 98.60, 104.27, 107.94, 108.63, 112.53, 117.38, 117.82, 119.31, 123.37, 123.89, 124.69, 124.78, 125.57, 125.60, 127.79, 128.54, 129.50, 129.54, 132.92, 144.73, 145.61, 149.16, 151.56, 152.50, 153.35, 166.90.

# Results and discussion

### Synthesis and characterization of Rh-Ip-Hy

The synthesis procedure for the probe **Rh-Ip-Hy** is shown in Scheme 2. First, compound **1** was prepared according to the

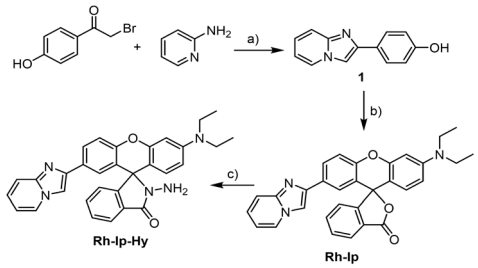


**Scheme 2** Synthesis routes of **Rh-Ip-Hy**. Reagents and conditions: a) $Na_2CO_3$, EtOH, reflux for 20 h; b) 2-(4-(*N*,*N*-diethylamino)-2-hydroxybenzoyl)benzoic acid, TFA/$MeSO_3H$ (v/v, 1/1), 80 °C for 24 h; c) hydrazine hydrate, EtOH, 100 °C for 4 h.

literature[22] by the reaction of 2-bromo-1-(4-hydroxyphenyl) ethanone with 2-aminopyridine and was allowed to react with 2-(4-(*N*,*N*-diethylamino)-2-hydroxyben-zoyl)benzoic acid according to a conveniently acid-promoted Friedel–Crafts acylation protocol in $CF_3COOH/CH_3SO_3H$ (v/v, 1/1) to produce **Rh-Ip**. Subsequently, the target probe **Rh-Ip-Hy** was prepared with a yield of 50% through the reaction of **Rh-Ip** with hydrazine hydrate in anhydrous ethanol. The structures of **Rh-Ip** and **Rh-Ip-Hy** were characterized using high-resolution mass spectrometry (HRMS) and $^1$H- and $^{13}$C-NMR spectroscopy (see the ESI†).

## Sensing performance of the probe for mercury ions

To determine the appropriate solvent environment for the interaction of **Rh-Ip-Hy** and $Hg^{2+}$, the fluorescence response of **Rh-Ip-Hy** towards $Hg^{2+}$ was determined in mixtures of water and different organic solvents (v/v, $H_2O$/organic solvent = 4/1). As shown in Fig. S1,† after the addition of $Hg^{2+}$ to the probe solutions, no obvious emission changes were observed in DMF/$H_2O$, DMSO/$H_2O$, and $CH_3CN/H_2O$ systems. In contrast, there was a significant fluorescence enhancement in the EtOH/$H_2O$ system, indicating interactions between **Rh-Ip-Hy** and $Hg^{2+}$. Therefore, the EtOH/$H_2O$ (v/v, 1/4) solvent system was chosen to investigate the spectral response of the probe to $Hg^{2+}$.

Firstly, the spectra of **Rh-Ip-Hy** (5 μM) after adding increasing amounts of mercury ions in PBS buffer (10 mM, EtOH/$H_2O$ = 1/4, pH 7.4) were investigated. As shown in Fig. 1a, the probe **Rh-Ip-Hy** exhibited almost no absorption within the range of 400–700 nm, which is attributed to the closed ring structure of the spirolactam. After the addition of $Hg^{2+}$ (0–80 μM), the absorbance of the probe at 500 nm gradually increased with the increasing concentrations of $Hg^{2+}$, indicating that $Hg^{2+}$ induced the ring-opening form of **Rh-Ip-Hy** (Scheme 1B). For fluorescence titration, as shown in Fig. 1b, the gradual addition of $Hg^{2+}$ to the probe solution resulted in an increased emission band at 575 nm, which reached the maximum and remained stable when the concentration of $Hg^{2+}$ ions exceeded 50 μM. The data

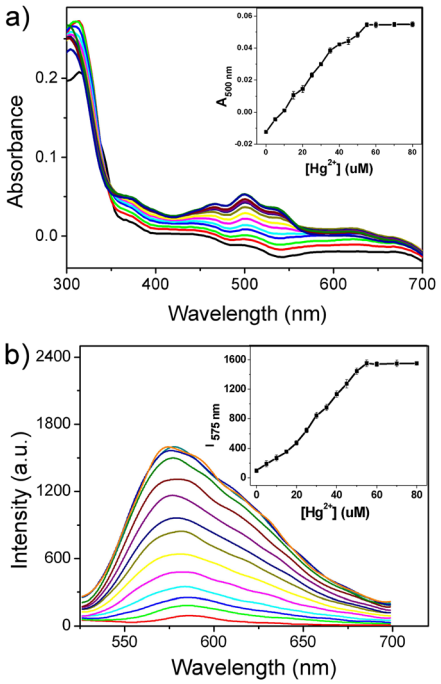


**Fig. 1** a) UV–vis and b) fluorescence spectra of **Rh-Ip-Hy** (5 μM) after adding increasing amounts of $Hg^{2+}$ in the PBS buffer (10 mM, EtOH/$H_2O$ = 1/4, pH of 7.4). Insets: the corresponding intensity changes of the probe as a function of $Hg^{2+}$ concentration.

suggested that the interactions between the probe and the $Hg^{2+}$ ions led to a colored and fluorescent compound (Scheme 1B). Furthermore, **Rh-Ip-Hy** exhibited a larger Stokes shift (75 nm) than the classic rhodamine and fluorescein dyes with a typical Stokes shift of less than 30 nm, which could reduce self-absorption and prevent self-quenching from excitation light. A linear relationship was observed between the fluorescence intensities of **Rh-Ip-Hy** and $Hg^{2+}$ within the concentration range of 0–50 μM. The detection limit of $Hg^{2+}$ ions was found to be 57.57 nM ($R^2$ = 0.9981, $\sigma$ = 0.6094, $k$ = 3.176 × $10^7$, $n$ = 10) based on 3 times the standard deviation rule (Fig. S2†).

Then, the spectral properties of **Rh-Ip-Hy** in the absence and presence of various metal ions were investigated. As shown in Fig. 2a, **Rh-Ip-Hy** (5 μM) showed almost no emission beyond 500 nm, indicating the closed spirolactam ring structure of the probe. After the addition of various metal ions (50 μM) including $Ag^+$, $Al^{3+}$, $Ca^{2+}$, $Cd^{2+}$, $Co^{2+}$, $Cu^{2+}$, $Fe^{3+}$, $Fe^{2+}$, $K^+$, $Li^+$, $Mg^{2+}$, $Mn^{2+}$, $Na^+$, $Ni^+$, $Pb^{2+}$, and $Zn^{2+}$ to the solution of the probe, no significant emission changes were observed. In contrast, the addition of $Hg^{2+}$ triggered a distinct emission intensity increase at 575 nm, with a more than 20-fold enhancement in the intensity. Since some spirolactam-based xanthene probes have been reported to react with $ClO^-$ or other reactive oxygen species (ROS),[23–25] the effect of ROS on the fluorescence of **Rh-Ip-Hy** was also investigated. As shown in Fig. 2a, the addition of ROS (including $H_2O_2$, NaClO, and ·OH) did not produce any obvious changes in the fluorescence of the probe. The

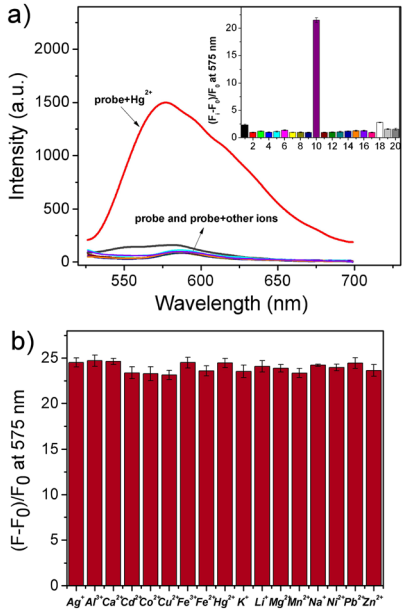


Fig. 2 a) Fluorescence spectra of **Rh-Ip-Hy** (5 μM) in the presence of 50 μM of various interfering species. Inset: histogram representing the fluorescence enhancement of the probe at 575 nm in the presence of various interfering species. 1: probe, 2: $Cu^{2+}$, 3: $Ag^{+}$, 4: $Fe^{2+}$, 5: $Zn^{2+}$, 6: $Pb^{2+}$, 7: $Ni^{2+}$, 8: $Mg^{2+}$, 9: $Al^{3+}$, 10: $Hg^{2+}$, 11: $Co^{2+}$, 12: $Cd^{2+}$, 13: $Ca^{2+}$, 14: $Ba^{2+}$, 15: $K^{+}$, 16: $Fe^{3+}$, 17: $Li^{+}$, 18: $ClO^{-}$, 19: $H_2O_2$, and 20: ·OH; b) changes $((F_i - F_0)/F_0)$ in the fluorescence intensity (575 nm) of the probe (5 μM) upon the addition of each metal ion (50 μM) followed by $Hg^{2+}$ (50 μM). $\lambda_{ex}$: 500 nm. Slit: 10 nm, 10 nm.

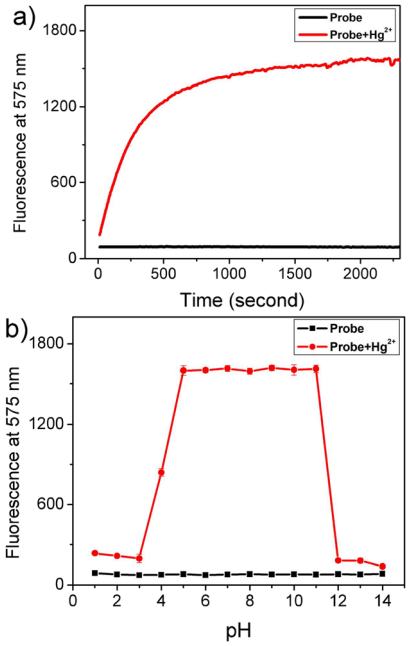


Fig. 3 a) Time-dependent fluorescence change (at 575 nm) of **Rh-Ip-Hy** (5 μM) with the addition of $Hg^{2+}$ (10 equiv.) in the PBS buffer solution (10 mM, EtOH/$H_2O$ = 1/4, pH of 7.4). b) Profile of pH dependence of the fluorescence intensity of the probe (5 μM) at 575 nm in the absence and presence of $Hg^{2+}$ (10 equiv.) in the PBS buffer solution (10 mM, EtOH/$H_2O$ = 1/4).

results indicated the high selectivity of **Rh-Ip-Hy** to $Hg^{2+}$ among various metal ions. Furthermore, the anti-interference experiment revealed that other metal ions did not have any significant effect on the sensing of mercury ions by the probe (Fig. 2b). These results suggested that **Rh-Ip-Hy** could be employed as a tool for tracing $Hg^{2+}$ in biological samples.

For practical and bioimaging applications, the time-dependent fluorescence responses of **Rh-Ip-Hy** to $Hg^{2+}$ were recorded. As shown in Fig. 3a, the addition of $Hg^{2+}$ to the solution of the probe induced a significant fluorescence enhancement at 575 nm within the first 10 min. The fluorescence gradually stabilized within 30 min, indicating the reaction equilibrium between the probe and the $Hg^{2+}$ ions. Then, experiments to assess the pH dependency of the fluorescence were conducted in the presence and absence of $Hg^{2+}$. As shown in Fig. 3b, the probe exhibited weak fluorescence within the pH range of 1–14, which was attributed to the closed spirolactam ring structure of the probe. Compared with many reported spirolactam ring structure probes,[26,27] the probe **Rh-Ip-Hy** exhibited high pH tolerance (Table S1†). After the addition of $Hg^{2+}$, the probe exhibited an obvious and stable fluorescence enhancement at 575 nm in the pH range of 5–11. These results showed that **Rh-Ip-Hy** could detect mercury ions within a wide pH range (5.0–11.0), which also covers the physiological pH conditions.

## Investigation of the sensing mechanism

To elucidate the sensing mechanism of **Rh-Ip-Hy** for $Hg^{2+}$, HRMS of the probe before and after its reaction with $Hg^{2+}$ was conducted. As shown in Fig. S3a,† the probe alone exhibited a peak at (*m*/*z*) 502.22, which corresponds to the **Rh-Ip-Hy** $[M + H]^+$ ion (calcd.: 502.22). After reacting with three equivalents of $Hg^{2+}$ for 20 min, the intensity of the peak at (*m*/*z*) 502.22 was considerably lower, and a new peak was observed at (*m*/*z*) 488.19, which corresponds to the hydrolyzed product of **Rh-Ip** (Fig. S3b†). Based on the HRMS results, we therefore suggest that the fluorescence of the probe can be switched on and off because of the selective $Hg^{2+}$-promoted opening of the spirolactam ring and the subsequent hydrolysis process (Scheme 3). Similar reaction mechanisms have also been reported in previous studies.[28–32]

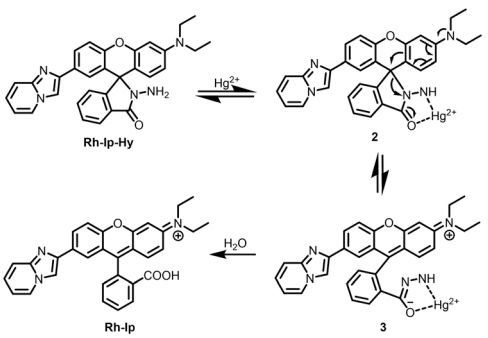


Scheme 3 Suggested recognition mechanism of **Rh-Ip-Hy** for $Hg^{2+}$.

### Application in cell imaging

To further explore the potential biological properties of **Rh-Ip-Hy**, its cytotoxicity to HeLa cells was evaluated using the CCK-8 assay. As shown in Fig. 4, after co-incubation with the probe (40 μM) for 24 hours, the survival rate of the cells was greater than 80%, which indicated that the probe had low cytotoxicity to cells and could be used for bio-imaging. Cell imaging for $Hg^{2+}$ was conducted using **Rh-Ip-Hy** as a tracer. As shown in Fig. 5, the HeLa cells incubated with the probe (5 μM) exhibited almost no fluorescence in the green channel (500–550 nm). However, significant and increased fluorescence was observed when the above-mentioned cells were treated with 2 equivalents of $Hg^{2+}$. These results demonstrated that **Rh-Ip-Hy** can permeate the cell and be used as a tracer for the detection of mercury ions in living cells.

### Detection of $Hg^{2+}$ with paper strips in real water samples

To facilitate the convenient on-site use of the fluorescence method, test strips were prepared by immersing filter paper strips into an ethanolic solution of **Rh-Ip-Hy** (100 μM) for 1 h. The strips were then dried with a blow-dryer. $Hg^{2+}$ solutions of different concentrations (0, 100, 150, 200, and 250 μM) were dropwise pipetted onto the dried paper strips.

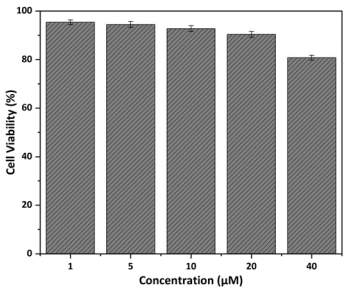


Fig. 4 Cell viability of HeLa cells after incubation with different concentrations of **Rh-Ip-Hy** for 12 hours.

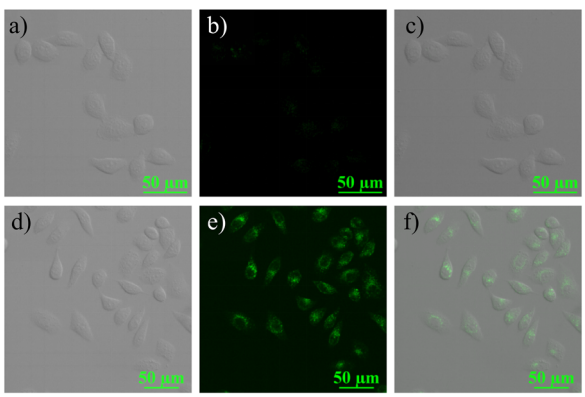


Fig. 5 Confocal fluorescence images of HeLa cells. a–c) Brightfield, fluorescence and merged images of HeLa cells after incubation with **Rh-Ip-Hy** (5 μM) for 30 min. d–f) Brightfield, fluorescence and merged images of HeLa cells pretreated with **Rh-Ip-Hy** (5 μM) for 30 min, and then incubated with $Hg^{2+}$ (10 μM) for 20 min.

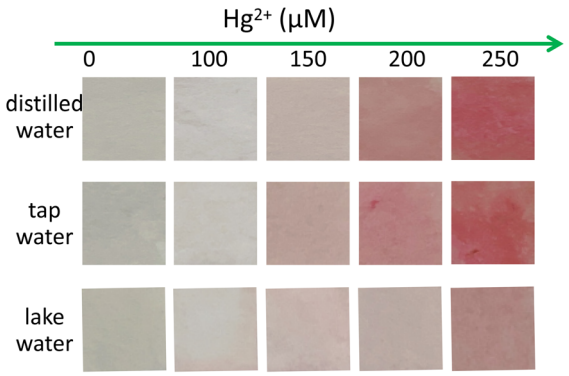


Fig. 6 Visualization of $Hg^{2+}$ using the test strips prepared with **Rh-Ip-Hy** in distilled water, tap water and lake water, respectively.

After natural drying, the color changes in the paper strips were observed under natural light. As shown in Fig. 6, the addition of $Hg^{2+}$ induced noticeable color changes in the paper strips from sage green to red under natural light. Furthermore, the colors of the strips deepened with the increase in the concentration of $Hg^{2+}$. When the test strips were used for sensing $Hg^{2+}$-containing tap water or lake water, similar color changes were observed (Fig. 6). These results indicated that test strips with **Rh-Ip-Hy** as a probe can be easily prepared for the simple and convenient detection of $Hg^{2+}$ in real water samples.

## Conclusions

In summary, an imidazo[1,2-*a*]pyridine-functionalized xanthene fluorescent probe (**Rh-Ip-Hy**) was designed and prepared for detecting $Hg^{2+}$ in various environments. Due to its asymmetric structure, the probe shows a larger Stokes shift (75 nm) than the classic rhodamine and fluorescein dyes. Because of the presence of a Lewis base site, the probe maintains a nonfluorescent ring-closed spirolactam structure within the pH range of 1–14, and shows selective fluorescence off–on signals to $Hg^{2+}$ within a wide pH-response range (5–11). **Rh-Ip-Hy** can permeate the cell membrane and can be used for the imaging of $Hg^{2+}$ in HeLa cells. Finally, **Rh-Ip-Hy**-loaded strips can be easily prepared and exhibit good performance for the detection of $Hg^{2+}$ in various water samples.

## Conflicts of interest

There are no conflicts to declare.

## Acknowledgements

We gratefully acknowledge the National Natural Science Foundation of China (Grant No. 22274068, 22076073), the Major Basic Research Project of Natural Science Foundation of Shandong Province (No. ZR2023ZD27) and the Natural Science Foundation of Shandong Province (No. ZR2022QB123).

## Notes and references

1 N. Sridhara Chary, C. T. Kamala and D. S. Suman Raj, *Ecotoxicol. Environ. Saf.*, 2008, **69**, 513–524.
2 A. Renzoni, F. Zino and E. Franchi, *Environ. Res.*, 1998, **77**, 68–72.
3 M. Harada, *Crit. Rev. Toxicol.*, 1995, **25**, 1–25.
4 N. Basu, A. Scheuhammer, N. Grochowina, K. Klenavic, F. Evans, M. Obrien and M. Chan, *Environ. Sci. Technol.*, 2005, **39**, 3585–3591.
5 J. R. Miranda-Andrades, S. Khan, M. J. Pedrozo-Penãfiel, K. de C. B. Alexandre, R. M. Maciel, R. Escalfoni, M. L. B. Tristão and R. Q. Aucelio, *Spectrochim. Acta, Part B*, 2019, **158**, 105641.
6 R. A. Bernhoft, *J. Environ. Public Health*, 2012, **2012**, 460508.
7 X. Chen, T. Pradhan, F. Wang, J. S. Kim and J. Yoon, *Chem. Rev.*, 2012, **112**, 1910–1956.
8 J. F. Zhang, Y. Zhou, J. Yoon and J. S. Kim, *Chem. Soc. Rev.*, 2011, **40**, 3416–3429.
9 K. Ponnuvel, V. Padmini and R. Sribalan, *Sens. Actuators, B*, 2016, **222**, 605–611.
10 K. Ponnuvel, M. Kumar and V. Padmini, *Sens. Actuators, B*, 2016, **227**, 242–247.
11 Y. Tian, Z. Zhou, J. Gong, J. Li, C. He and J. Chen, *Sens. Actuators, B*, 2023, **394**, 134421.
12 R. Zou, Y. Yu, H. Pan, P. Zhang, F. Cheng and C. Zhang, *ACS Appl. Mater. Interfaces*, 2022, **14**, 16746–16754.
13 H. Liu, P. Zhang, C. Zhang, J. Chen and J. H. Jiang, *ACS Appl. Mater. Interfaces*, 2020, **12**, 45822–45829.
14 P. Zhang, X. Nie, M. Gao, F. Zeng, A. Qin, S. Wu and B. Z. Tang, *Mater. Chem. Front.*, 2017, **1**, 838–845.
15 H. N. Kim, M. H. Lee, H. J. Kim, J. S. Kim and J. Yoon, *Chem. Soc. Rev.*, 2008, **37**, 1465–1472.
16 H. Zheng, X. Q. Zhan, Q. N. Bian and X. J. Zhang, *Chem. Commun.*, 2013, **49**, 429–447.
17 P. Zhang, Y. Tian, H. Liu, J. Ren, H. Wang and R. Zeng, *Chem. Commun.*, 2018, **54**, 7231–7234.
18 Z. Tian, B. Tian and J. Zhang, *Dyes Pigm.*, 2013, **99**, 1132–1136.
19 Z. Zhang, G. Zhang, J. Wang, S. Sun and Z. Zhang, *Comput. Theor. Chem.*, 2016, **1095**, 44–53.
20 S. Samanta, K. Lai, F. Wu, Y. Liu, S. Cai, X. Yang, J. Qu and Z. Yang, *Chem. Soc. Rev.*, 2023, **52**, 7197–7261.
21 B. Wang, S. Yu, X. Chai, T. Li, Q. Wu and T. Wang, *Chem. – Eur. J.*, 2016, **22**, 5649–5656.
22 M. Leopoldo, E. Lacivita, E. Passafiume, M. Contino, N. A. Colabufo, F. Berardi and R. Perrone, *J. Med. Chem.*, 2007, **50**, 5043–5047.
23 M. Ren, B. Deng, K. Zhou, X. Kong, J. Y. Wang, G. Xu and W. Lin, *J. Mater. Chem. B*, 2016, **4**, 4739–4745.
24 R. Bhowmick, A. S. M. Islam, U. Saha, G. S. Kumar and M. Ali, *New J. Chem.*, 2018, **42**, 3435–3443.
25 X. Chen, X. Wang, S. Wang, W. Shi, K. Wang and H. Ma, *Chem. – Eur. J.*, 2008, **14**, 4719–4724.
26 C. Yu, J. Zhang, J. Li, P. Liu, P. Wei and L. Chen, *Microchim. Acta*, 2011, **174**, 247–255.
27 S. Das, K. Rissanen and P. Sahoo, *ACS Omega*, 2019, **4**, 5270–5274.
28 D. Li, C. Y. Li, Y. F. Li, Z. Li and F. Xu, *Anal. Chim. Acta*, 2016, **934**, 218–225.
29 Q. Zhang, H. Ding, X. Xu, H. Wang, G. Liu and S. Pu, *Spectrochim. Acta, Part A*, 2022, **276**, 121242.
30 K. Huang, Y. Liu, P. Zhao, L. Liang, Q. Wang and D. Qin, *Spectrochim. Acta, Part A*, 2022, **282**, 121688.
31 X. Jiao, C. Liu, K. Huang, S. Zhang, S. He, L. Zhao and X. Zeng, *Org. Biomol. Chem.*, 2015, **13**, 6647–6653.
32 Y. Zhao, Y. Ren, H. Li, T. Han, H. Chen and W. Guo, *Dyes Pigm.*, 2016, **132**, 255–261.